10-20-2023

What caused the unseasonal extreme dust storm in Uzbekistan during November 2021?

Xin Xi
Michigan Technological University, xinxi@mtu.edu

Daniel Steinfeld
University of Bern

Steven M. Cavallo
The University of Oklahoma

Jun Wang
University of Iowa, Center for Global and Regional Environmental Research

Jiquan Chen
Michigan State University

See next page for additional authors

Recommended Citation

Xi, X., Steinfeld, D., Cavallo, S., Wang, J., Chen, J., Zulpykharov, K., & Henebry, G. (2023). What caused the unseasonal extreme dust storm in Uzbekistan during November 2021?. *Environmental Research Letters, 18*(11). http://doi.org/10.1088/1748-9326/ad02af
Retrieved from: https://digitalcommons.mtu.edu/michigantech-p2/464

Follow this and additional works at: https://digitalcommons.mtu.edu/michigantech-p2

 Part of the Geological Engineering Commons, and the Mining Engineering Commons

ENVIRONMENTAL RESEARCH
LETTERS

LETTER • OPEN ACCESS

What caused the unseasonal extreme dust storm in Uzbekistan during November 2021?

To cite this article: Xin Xi *et al* 2023 *Environ. Res. Lett.* **18** 114029

IOP Publishing Environ. Res. Lett. 18 (2023) 114029 https://doi.org/10.1088/1748-9326/ad02af

ENVIRONMENTAL RESEARCH
LETTERS

OPEN ACCESS

RECEIVED
24 August 2023

REVISED
4 October 2023

ACCEPTED FOR PUBLICATION
12 October 2023

PUBLISHED
20 October 2023

LETTER

What caused the unseasonal extreme dust storm in Uzbekistan during November 2021?

Xin Xi[1,*], Daniel Steinfeld[2], Steven M Cavallo[3], Jun Wang[4], Jiquan Chen[5,6], Kanat Zulpykharov[7] and Geoffrey M Henebry[5,6]

[1] Department of Geological and Mining Engineering and Sciences, Michigan Technological University, Houghton, MI, United States of America
[2] Institute of Geography and Oeschger Centre for Climate Change Research, University of Bern, Bern, Switzerland
[3] School of Meteorology, University of Oklahoma, Norman, OK, United States of America
[4] Department of Chemical and Biochemical Engineering, Center for Global and Regional Environmental Research and Iowa Technology Institute, The University of Iowa, Iowa City, IA, United States of America
[5] Department of Geography, Environment, and Spatial Sciences, Michigan State University, East Lansing, MI, United States of America
[6] Center for Global Change and Earth Observations, Michigan State University, East Lansing, MI, United States of America
[7] Department of Geography and Environmental Sciences, Al-Farabi Kazakh National University, Almaty, Kazakhstan
[*] Author to whom any correspondence should be addressed.

E-mail: xinxi@mtu.edu

Keywords: extreme event, dust storm, cold air outbreak, La Niña, Central Asia

Supplementary material for this article is available online

Abstract

An unseasonal dust storm hit large parts of Central Asia on 4–5 November 2021, setting records for the column aerosol burden and fine particulate concentration in Tashkent, Uzbekistan. The dust event originated from an agropastoral region in southern Kazakhstan, where the soil erodibility was enhanced by a prolonged agricultural drought resulting from La Niña-related precipitation deficit and persistent high atmospheric evaporative demand. The dust outbreak was triggered by sustained postfrontal northerly winds during an extreme cold air outbreak. The cold air and dust outbreaks were preceded by a chain of processes consisting of recurrent synoptic-scale transient Rossby wave packets over the North Pacific and North Atlantic, upper-level wave breaking and blocking over Greenland, followed by high-latitude blocking over Northern Europe and West Siberia, and the equatorward shift of a tropopause polar vortex and cold pool into southern Kazakhstan. Our study suggests that the historic dust storm in Uzbekistan was a compound weather event driven by cold extreme, high winds, and drought precondition.

1. Introduction

On 4–5 November 2021, an extreme dust storm hit large parts of Uzbekistan, Tajikistan, and Turkmenistan, causing property damage, socioeconomic disruption, and a surge of respiratory illnesses. The event has been described in the media as the worst dust storm ever recorded in Uzbekistan. Tashkent, the most populous city of Central Asia, reportedly suffered extremely high concentrations of fine particulates ($PM_{2.5}$) resulting in an increase of acute respiratory problems and ambulance service calls [1]. Poor visibility and hazardous weather also caused automobile accidents and power outages in surrounding regions [1].

Climatologically, dust outbreaks in Central Asia are most common between late spring and early summer due to frequent cold intrusion from high latitudes and sufficiently dry and exposed soils during the early growing season [2, 3]. The 2021 November dust event was a rare occurrence during the boreal cold season, when dust emission is usually suppressed by seasonally high precipitation and possible early onset of snow cover [4]. The event was reportedly triggered by a cold air outbreak (CAO) linked to the Siberian High, which was found to extend abnormally westward to the Caspian Sea from its typical center of action during winter 2021 [5]. The CAO reportedly triggered record snowfall and persistent cold extremes across China during 6–8 November

2021 [6, 7]. In addition, Central Asia suffered severe drought and record high temperatures in 2021, which may have enhanced the soil erodibility and susceptibility to wind erosion [8].

While past studies shed some light on the meteorological aspect of the unseasonal dust storm in Uzbekistan, several key questions remain unanswered, including: (1) how intense was the dust storm from a climatological perspective? (2) What atmospheric processes triggered the cold air and dust outbreaks? and (3) how did the regional hydroclimate contribute to the dust outbreak? This study presents observational evidence of the record-breaking aerosol burden and particulate pollution following the dust outbreak (section 3.1), and investigates the atmospheric dynamics (section 3.2) and hydroclimate preconditions (section 3.3) associated with such an unseasonal extreme dust event in Central Asia.

2. Data and methods

Two long-term observations are used to evaluate the dust event intensity in Tashkent: Hourly $PM_{2.5}$ concentration and Air Quality Index reported from the U.S. Embassy in Tashkent, and daily average coarse-mode aerosol optical depth (AOD 550 nm) derived from the Moderate Resolution Imaging Spectroradiometer (MODIS) level 2 deep-blue and dark-target merged AOD and fine mode fraction [9]. Surface synoptic observations and ERA5 reanalysis are used to investigate the precursory atmospheric processes leading up to the dust outbreak. Specifically, we identify two upper-level dynamical features related to persistent high-impact surface weather: atmospheric blocking and recurrent synoptic-scale transient Rossby wave packets. Blocks are defined as regions with persistent negative anomalies of 500–150 hPa vertically averaged potential vorticity (PV) exceeding -1.3 PVU ($1\,\mathrm{PVU} = 10^{-6}\,\mathrm{Km^2\,s^{-1}\,kg^{-1}}$) and a spatial overlap of at least 70% between successive 6 hourly time steps for at least 5 days [10, 11]. Recurrent Rossby wave packets can repeatedly pass and amplify at the same longitude in the same phase, resulting in recurring ridging or troughing patterns and persistent cold or hot extremes [12, 13]. The strength of the transient Rossby wave packets is described by a 'R' metric, which is a time- and wavenumber-filtered signal derived from the Hovmöller diagram of 250 hPa meridional winds averaged over 35° N–65° N [14].

In addition, we examine the role of tropopause polar vortices (TPVs) in the CAO development using the TPVTrack method [15]. TPVs are subsynoptic-scale, coherent tropopause-based vortices with typical radii of 100 to 1000 km and lifetimes of days to months, characterized by a local minimum of dynamic tropopause potential temperature, a cyclonic PV anomaly in the Arctic lower stratosphere, and a lowered tropopause often to the 500 hPa level or below [16–18]. The equatorward advection of TPVs and associated cold pool can trigger intense CAOs in the midlatitudes [19–21]. Finally, we assess the drought severity and impact on the soil erodibility using three long-term datasets, including the Climate Research Unit Time Series monthly precipitation and potential evapotranspiration (PET) [22], European Space Agency Climate Change Initiative blended passive-active microwave soil moisture product [23, 24], and MODIS Climate Modeling Grid global level 3 monthly Normalized Difference Vegetation Index (NDVI) product [25]. The microwave soil moisture product represents the top 2 cm of the soil and is thus closely related to the inter-particle cohesion and wind erodibility of top soil [26].

3. Results

3.1. Observed extreme dust burden in Tashkent

According to geostationary satellite observations, the initial dust outbreak began around 03:30Z (08:30 AM) 4 November 2021 from an agropastoral area in the Ordabasy District of southern Kazakhstan (see figure S1 for details). The source area consisted of a mix of semiarid steppe (used as natural pasture) and rainfed croplands near the lower Arys River. Three hours later, MODIS onboard Terra detected a cone-shaped dust plume advancing south (figure 1(a)) and sweeping across several highly populated regions the next day (figure 1(b)), including the Fergana Valley, Gissar Valley, and the foothills of Tien Shan–Pamirs mountains. Located 150 km downwind, Tashkent experienced record-breaking particulate concentration and persistent unhealthy air quality following the dust outbreak (figure 1(c)). The U.S. Embassy at Tashkent observed a peak $PM_{2.5}$ concentration of 978 $\mu g\,m^{-3}$ on 5 November 2021 (figure 1(c)). It was the highest $PM_{2.5}$ ever observed across all U.S. Embassy locations in Central Asia (figure S2). The Centre of Hydrometeorological Service of Uzbekistan (Uzhydromet) reported even higher $PM_{2.5}$ levels in excess of 2000 $\mu g\,m^{-3}$ or 30 times the permissible level in Tashkent [27]. The extreme dust burden was also observed by the MODIS coarse-mode AOD record. Particularly, the dust storm caused the highest AOD in Tashkent during the boreal cold season (November–April), as well as the second highest annual mean AOD since 2001 (figure 1(d)).

3.2. Atmospheric dynamics of cold air and dust outbreaks

On 4 November 2021, surface synoptic observations near the dust source revealed a reversal and rapid rise of sea level pressure, a sudden drop of temperature, and a shift from calm condition to sustained northerly winds (figure 2(a)), which collectively indicated the passage of a cold front. Persistent wind gusts of

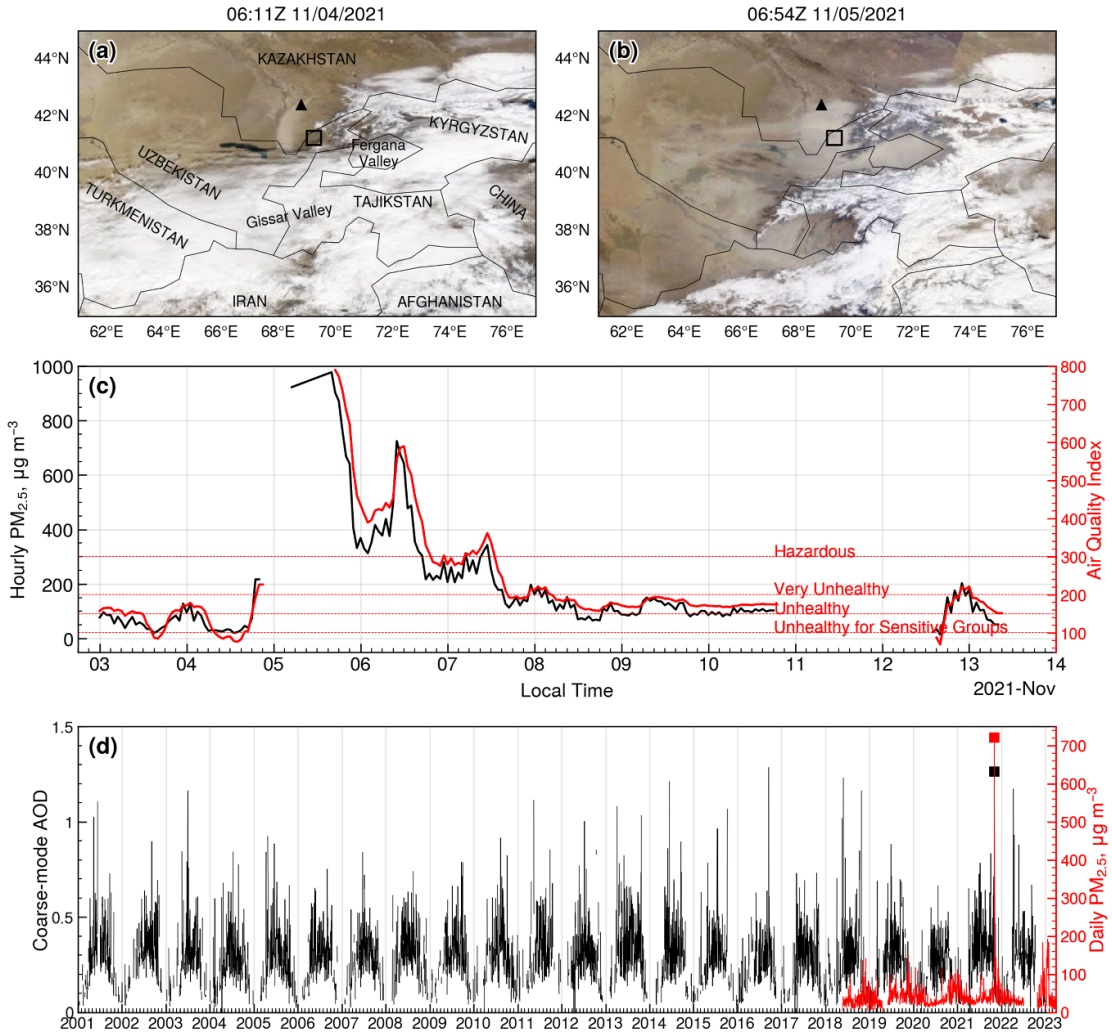

Figure 1. (a), (b) MODIS/Terra true color images on 4 and 5 November 2021. Black triangles denote the weather station at Arys, Kazakhstan. Open squares denote the geographic domain for computing the regional mean AOD over Tashkent. (c) Hourly $PM_{2.5}$ and Air Quality Index reported at the U.S. Embassy in Tashkent. Horizontal red lines are the unhealthy for sensitive groups, unhealthy, very unhealthy, and hazardous levels. (d) Daily average coarse-mode AOD and $PM_{2.5}$ in Tashkent. Observed values on 5 November 2021 are marked (AOD in black square; $PM_{2.5}$ in red square).

17–20 m s^{-1} triggered dust deflation which lowered the visibility to as low as 200 m. The sudden cooling was identified as a CAO event wherein the daily average temperature fell below 1.5 standard deviations of the 31 day running mean while the standard deviation exceeded 2 K [28]. The CAO spatial extent and intensity is shown in figure 2(b) which exhibits a pool of exceptionally cold airmass (i.e. 1000–500 hPa thickness below 510 dam) extending from the Arctic into Central Asia. As the polar air moved into southern Kazakhstan, the 1000–500 hPa thickness reached record low levels, with an extensive area falling below the 4th percentile of the 1960–2021 daily climatology.

What caused the extreme Arctic CAO? Figure 2(c) shows persistent, highly amplified meridional flows during the preceding month, consisting of multiple successive ridges and troughs forming recurrent transient synoptic-scale Rossby wave packets over the North Pacific and North Atlantic. The repeated meridional flow amplification was accompanied by frequent Rossby wave breaking (RWB) and blocking development. Particularly, persistent high-latitude blocking near Greenland (B1) since mid-October fostered high-amplitude recurrent Rossby waves over the eastern North Atlantic and subsequent formation of midlatitude blocking over Europe in late October, followed by high-latitude blocking over the Ural-Siberia region (B2) in early November just prior to the cold air and dust outbreaks.

The atmospheric blocking and CAO mechanisms are further examined using the dynamic tropopause potential temperature maps shown in figure 3. A high-amplitude ridge developed over northeastern Canada on 27 October 2021 (day −8), initiating RWB and blocking near Greenland (B1 in figure 3). A split flow pattern developed around the blocking

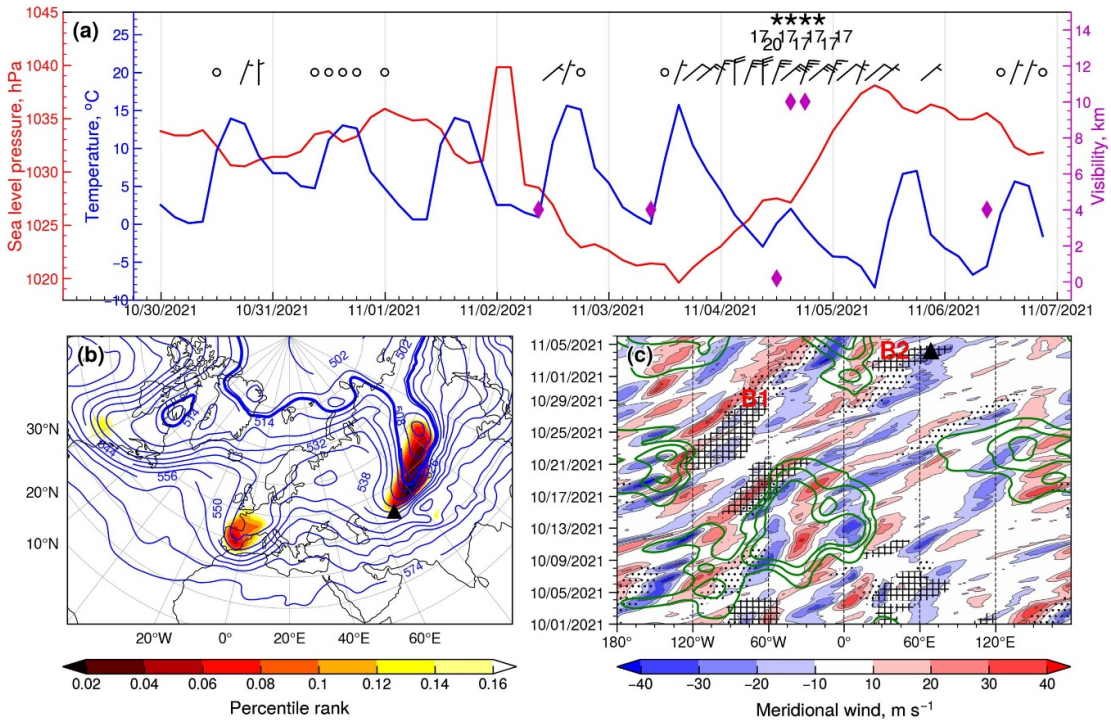

Figure 2. (a) Surface synoptic observations at Arys, Kazakhstan of sea level pressure (red line), temperature (blue line), visibility (diamonds), mean winds (wind barbs), maximum instantaneous wind speed (numbers; misaligned for clarity), and visual reports of dusty weather (asterisks). Local time is shown at the *x*-axis. (b) The 1000–500 hPa thickness on 4 November 2021 (contours every 6 dam; 510 dam in thick contours) and corresponding percentile rank within the 1960–2021 daily climatology (shading). (c) Hovmöller diagram of the 35° N–65° N averaged, 250 hPa meridional wind (shading), and R-metric values (green contours at 8, 10, and 12 m s^{-1}). Stippling (hatching) indicates the longitudes where at least 50% of the grid points within 45° N–60° N (60° N–75° N) feature an atmospheric block. Greenland (B1) and Ural (B2) blocking are marked. Black triangles in (b) and (c) indicate the weather station at Arys, Kazakhstan.

ridge and the October 2021 nor'easter located equatorward off the Mid-Atlantic coast (W). The meridional PV gradient intensified downstream in association with the superposition of the polar and subtropical jets (circled area in figure 3(a); see figure S3 for cross section along 45° W), driven by the simultaneous poleward transport of an anticyclonic PV anomaly in the warm sector of the nor'easter along the Gulf Stream and the equatorward incursion of a cyclonic PV anomaly from a TPV over the Lincoln Sea. A deep extratropical cyclone with a central pressure of 963 hPa (L) developed in the left exit region of the superposed jet, likely due to the strengthened ageostrophic transverse circulation in the jet exit and the polar cyclonic PV anomaly [29]. The warm sector of the extratropical low featured a poleward ascending flow of low PV air which favored upper-level ridging and block onset over Northern Europe (B2 in figure 3(b)) [30, 31]. As the amplifying ridge built into the Barents Sea, the Ural and West Siberia region experienced RWB, blocking onset, and formation of an elongated high PV trough (or PV streamer) downstream (figure 3(c)). The deepening trough was embedded with an equatorward shifted TPV which was situated near the Kara Sea two days earlier (see the TPV trajectory in figure 3(d)). The TPV experienced significant stretching and formed via splitting a new cyclonic coherent tropopause disturbance (CTD) over southern Kazakhstan (figure 3(d)).

The TPV and CTD were dynamically similar, with the difference being that the TPV formed and spent much of its lifetime in polar regions, which allows a tropospheric-deep cold pool to form within and underneath the TPV [18, 32]. Indeed, figure 3(e) shows that both the TPV and CTD featured a lowered tropopause to around 500 hPa and strong wind circulations surrounding them. The cold air triggering the CAO was associated with the TPV, as indicated by the isentropes bending upward into the TPV as well as the extremely low 1000–500 hPa thickness (figure 3(e)). The CTD formation in southern Kazakhstan, however, facilitated the deep penetration of the TPV-associated cold pool into the midlatitudes. At the ground level, the highest winds developed just behind the surface cold front (figures 3(e) and (f)), and ahead of rapid low-level anticyclogenesis (anticyclonic center denoted as H in figures 3(c) and (d)). Further analysis reveals that the anticyclonic center rose to 1050.6 hPa on 4 November at a rate of 8 hPa d^{-1}. The explosive anticyclogenesis and attendant sustained postfrontal northerly flows contributed to the intense dust outbreak in southern Kazakhstan and subsequent rapid dispersion to large parts of Central Asia (figure 2(b)).

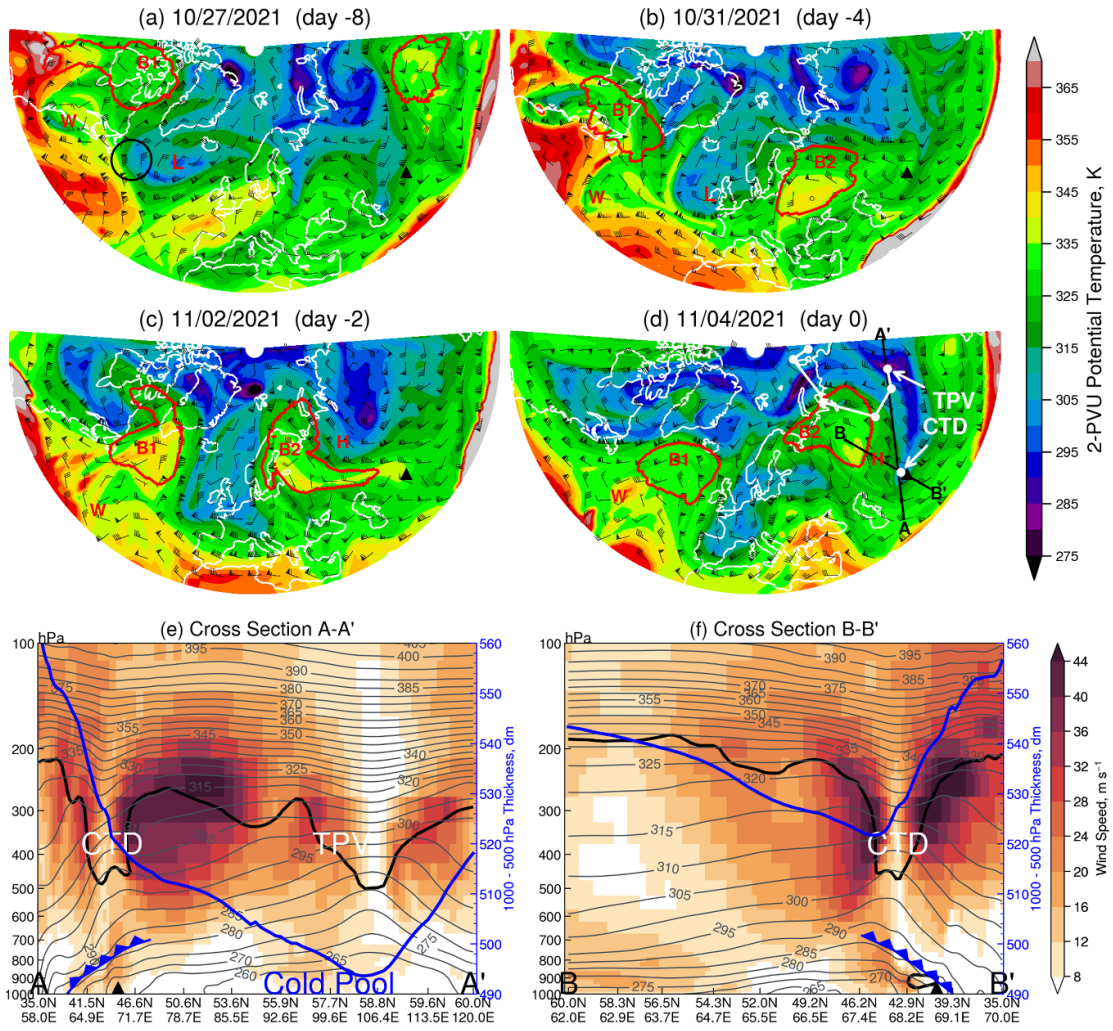

Figure 3. (a)–(d) Potential temperature (shading) and winds on the 2 PVU surface (or dynamic tropopause) at 06 UTC of preceding days of the dust storm. Major features are Greenland blocking (B1), Ural blocking (B2), October 2021 nor'easter which eventually became Tropical Storm Wanda (W), jet superposition (black circle), extratropical cyclogenesis (L), rapid anticyclogenesis (H), tropopause polar vortex (TPV), and coherent tropopause disturbance (CTD). The white dotted line in (d) denotes the TPV trajectory at 06 UTC between 30 October and 4 November 2021. (e), (f) Vertical cross sections of wind speed (shading) and potential temperature (gray contours every 5 K) along the A–A' and B–B' black lines in (d). The thick black contour denotes the dynamic tropopause. The thick blue contour denotes the 1000–500 hPa thickness. The approximate locations of surface cold front and TPV-associated cold pool are shown. The weather station at Arys, Kazakhstan is denoted as a black triangle in all panels.

The tropopause-level diagnosis suggests that the cold air and dust outbreaks were associated with blocking development over the Ural and West Siberia regions via a planetary wave train propagating from the North Atlantic. The wave propagation was supported by a strong meridional PV gradient at the Atlantic jet entrance region, but was followed by wave breaking directly downstream and poleward of the jet exit near Iceland (figure 3(a)). The upper-level wave breaking and blocking onset are closely related to changes in the Atlantic jet position, storm track, and leading patterns of the North Atlantic winter climate variability [34–37]. During the prior month of the dust storm (October 2021), frequent blocking accompanied by strong positive 500 hPa geopotential height anomalies occurred in the vicinity of Greenland, and to a lesser extent, over Northern Europe and West Siberia (figure 4(a)). Consistent with the high-latitude blocking, the eddy-driven polar jet shifted well southward into the subtropics over the central and eastern Atlantic (figure 4(a)). Based on the 1951–2020 climatology, extreme blocking conditions occurred near Greenland during October 2021, resulting in the second highest October Greenland Blocking Index (GBI) (2.3) since 1950 (figure 4(c)). The extreme positive GBI and associated equatorward shifted jet position corresponded to an exceptionally negative pattern of the North Atlantic Oscillation (NAO), as indicated by the second lowest October NAO score (−2.0) since 1950 (figure 4(c)). Extreme negative NAO and Greenland blocking favor enhanced meridional airmass transport contributing to more frequent CAOs over Eurasia and North America [38–41].

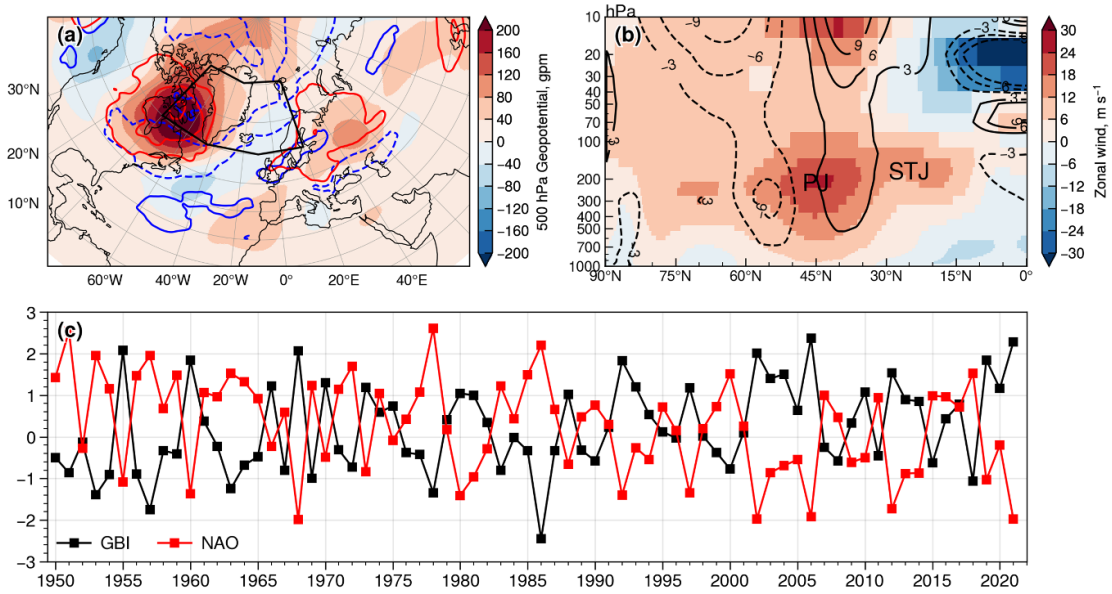

Figure 4. (a) 500 hPa geopotential height anomaly (shaded), 925–700 hPa averaged zonal wind anomaly (blue contours at −3 and 3 m s^{-1} with negative contours dashed), and blocking frequency (red contours at 10%, 30%, and 50%) during October 2021 (b) vertical cross section of the 0° W–60° W averaged zonal wind (shaded) and zonal wind anomaly (contours) during October 2021. PJ = polar front jet stream; STJ = subtropical jet stream. (c) Time series of October Greenland Blocking Index (GBI) and North Atlantic Oscillation (NAO). GBI is calculated as the normalized anomaly of the 500 hPa geopotential height averaged over 20° W–80° W, 60° N–80° N (boxed area in (a)) [33]. All anomalies are computed relative to 1951–2000.

3.3. Hydroclimate precondition and enhanced soil erodibility

While the CAO and attendant high winds triggered the dust outbreak onset, land surface conditions play an important role in modulating the location and intensity of dust emission, as indicated by the highly localized source activation despite the powerful frontal system (figure 1(a)). Notably, hydroclimate precondition, including soil moisture and vegetation, affects the aeolian sediment availability by increasing the soil inter-particle cohesion, sheltering dry or exposed surfaces, and reducing the near surface wind momentum through drag partition [4, 42]. Drought is an important precondition for increasing wind erosion in semiarid areas, and has been linked to previous intense dust periods in Central Asia [42, 43].

Central Asia suffered widespread precipitation declines in 2021, especially in the high mountains where most of the annual precipitation is received during the cold season and released as snowmelt runoff during the warm season (May–October) (figure 5(a)) [44, 45]. As the headwater area for the Arys river and surrounding agropastoral regions in southern Kazakhstan, western Tien Shan–Pamirs (boxed area in figure 5(a) received the lowest precipitation since 1990 (figure 5(e)). Meanwhile, the PET anomaly revealed persistent above-average atmospheric water demand (figure 5(b)), which exacerbated the already limited surface water. As a result, both the soil moisture and NDVI anomalies indicate widespread agricultural drought during the 2021 warm season (figures 5(c) and (d)). The severe drought reportedly caused massive crop failure and livestock deaths in Central Asia [8]. A closer look at the dust source region (boxed area in figures 5(c) and (d)) reveals prolonged drought conditions since 2019, which could result in a cumulative risk of desertification and wind erosion (figure 5(e)). In addition to drought, land use intensification from agricultural and pastoral productions may have further enhanced the sediment availability and localized dust emissions, as previously observed in southern Kazakhstan [43].

The recent prolonged drought of Central Asia occurred during a 'triple-dip' La Niña lasting for the past three winters of 2020–2023 (figure 5(e)). This unprecedented event continued the predominant multi-year La Niña and La Niña-like conditions since the turn of the century. A recent study suggested that La Niña events are associated with below-average precipitation during the cold season, below-average soil moisture and vegetation cover during the following warm season, and consequently above-average dust burden over Central Asia [43]. Previous studies also showed an increasing ENSO influence on the hydroclimate in Central Asia since the 1990 s, due to an increasing frequency of Central Pacific La Niña events characterized by anomalously cold central Pacific and warm western Pacific resulting in an enhanced zonal sea surface temperature (SST) gradient across the west Pacific (figure S4) [43, 46–51]. The seasonally persistent tropical thermal anomalies and zonal SST gradients foster coherent Rossby wave responses over East Africa and Central and Southwest Asia, often as part of a global zonal band of upper level

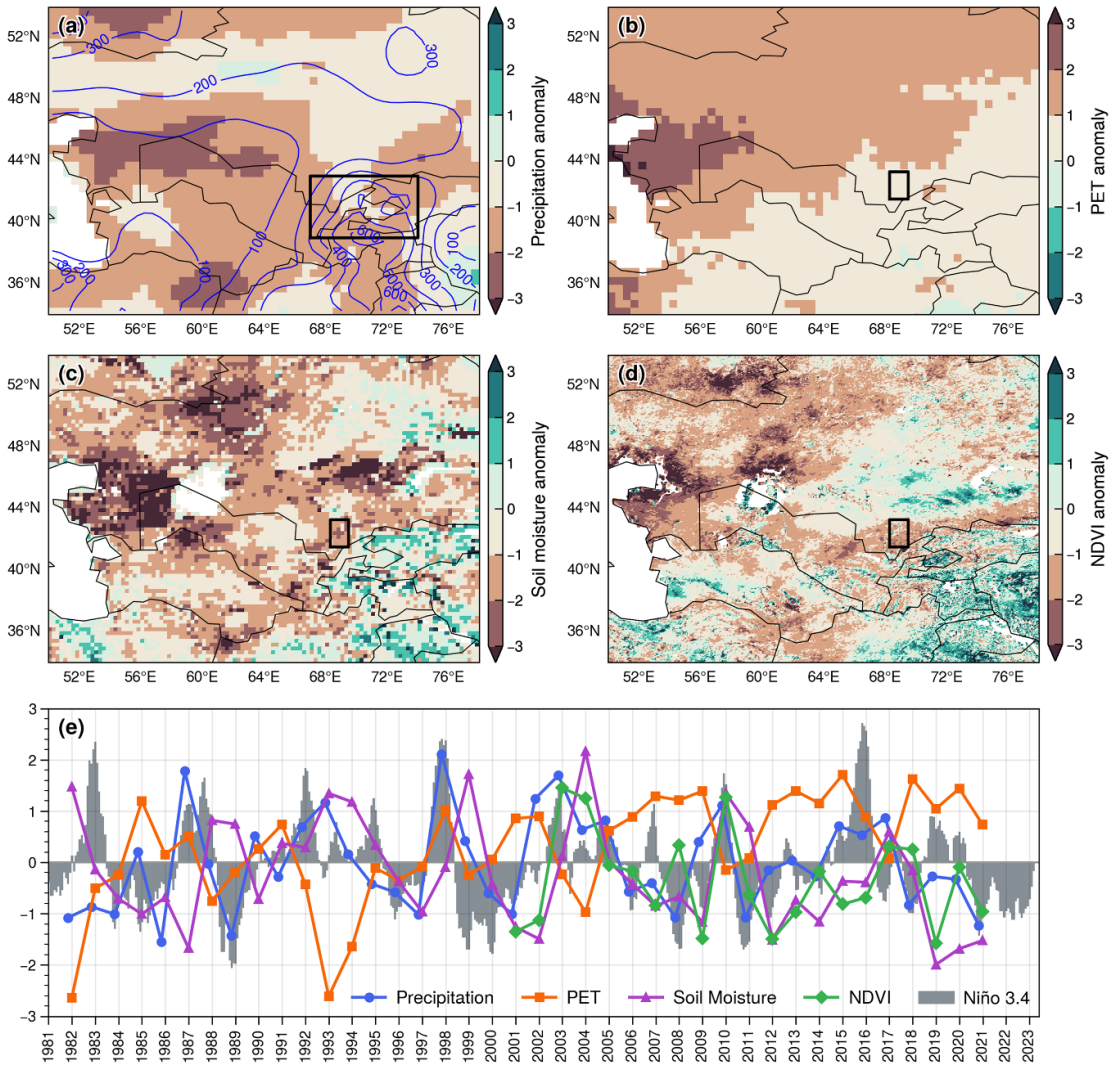

Figure 5. (a) The November 2020–October 2021 total precipitation (blue contours) and normalized anomaly relative to 1981–2010 (shaded). (b)–(d) The 2021 warm-season (May–October) anomalies of potential evapotranspiration (PET), soil moisture, and NDVI. (e) Regional mean anomalies of precipitation, PET, soil moisture, and NDVI over the boxed areas in (a)–(d) together with the monthly Niño 3.4 index. All anomalies are normalized relative to 1981–2010 except for NDVI (2001–2010).

anticyclonic anomalies leading to widespread precipitation reductions across the Northern Hemisphere midlatitudes (figures S5 and S6). The growing oceanic forcing of precipitation modifications over Central Asia has been largely attributed to the rapid warming and expansion of the tropical Indo-Pacific Ocean [52, 53].

4. Discussions and conclusions

The dust storm of 4–5 November 2021 in Uzbekistan, which originated from an agropastoral area of natural pasture and rainfed croplands in southern Kazakhstan, was an unseasonal extreme event with significant impact on regional air quality and socioeconomic activity. Our analysis suggests that this dust storm was a 'preconditioned' compound event caused by an extreme CAO and attendant postfrontal northerly winds (the driver) and a prolonged drought (the precondition) associated with a multi-year La Niña event (the driver of the precondition) [54]. The cold air and dust outbreaks were preceded by a succession of planetary- and synoptic-scale processes during the prior week, including recurrent transient synoptic-scale Rossby wave packets over the North Pacific, upper-level wave breaking and blocking near Greenland, southward shifted polar jet and extratropical cyclogenesis over the North Atlantic, and high-latitude blocking over Northern Europe and West Siberia. This type of Atlantic-origin wave train has been previously identified as a primary mechanism of CAOs in Asia [55–57]. Apart from the planetary waviness, the extreme CAO event was associated with the equatorward advection of an Arctic TPV and cold pools. While this case study is not sufficient to establish a causal link between TPV and CAO, equatorward shifted TPVs have been frequently associated with intense CAO events in mid- and low-latitude regions. For example, 40% of the most intense CAOs in the Fram Strait were associated with Arctic TPVs

[19], while TPVs were involved in 85% CAOs in eastern North America [21].

A prolonged agricultural drought—characterized by persistent below-average precipitation and above-average PET—desiccated the drylands of Central Asia, thereby creating a favorable precondition for dust uplifting from the dry, exposed soils. The severe drought was linked to an unprecedented 'triple-dip' La Niña event through teleconnection effect on the wintertime circulation and precipitation in Central Asia. Recent studies suggested that multi-year consecutive La Niña events, such as the recent occurrences of 2010–12, 2016–18, and 2020–23, may become more frequent under greenhouse warming [58]. The heightened risk of prolonged drought, combined with rising temperatures and atmospheric evaporative demand, may continue to aggravate the surface water availability, soil erodibility, and dust outbreaks in Central Asia.

Data availability statements

The data used in this study are publicly available from the following repositories: PM2.5 (www.airnow.gov/international/us-embassies-and-consulates/); MODIS AOD (https://search.earthdata.nasa.gov/); ECMWF ERA5 reanalysis (https://cds.climate.copernicus.eu); surface synoptic observations (www.ncei.noaa.gov/products/land-based-station/integrated-surface-database); SEVIRI Level 1.5 Image Data (https://navigator.eumetsat.int/product/EO:EUM:DAT:MSG:HRSEVIRI-IODC); MODIS NDVI (https://doi.org/10.5067/MODIS/MOD13C2.061); CRU TS dataset (https://crudata.uea.ac.uk/cru/data/hrg/); ESA CCI soil moisture (https://esa-soilmoisture-cci.org/); and climate indices (https://psl.noaa.gov/data/climateindices/list/). The blocking identification code ConTrack is available at https://github.com/steidani/ConTrack. Code for calculating the R metric is available at https://doi.org/10.5281/zenodo.5742810. The TPV tracking code tpvTrack is available at https://github.com/nickszap/tpvTrack.

Acknowledgments

X X and G M H acknowledge funding from the NASA Land Cover Land Use Change (LCLUC) program (80NSSC20K1480, 80NSSC20K0411) and Michigan Space Grant Consortium (SUBK00011994). D S acknowledges funding from the Wyss Academy for Nature. We thank two anonymous reviewers for their constructive suggestions and comments.

ORCID iDs

Xin Xi https://orcid.org/0000-0003-3804-2735
Daniel Steinfeld https://orcid.org/0000-0001-8525-4904
Jun Wang https://orcid.org/0000-0002-7334-0490
Jiquan Chen https://orcid.org/0000-0003-0761-9458
Geoffrey M Henebry https://orcid.org/0000-0002-8999-2709

References

[1] Broomandi P *et al* 2023 A synoptic-and remote sensing-based analysis of a severe dust storm event over Central Asia *Aerosol Air Qual. Res.* **23** 220309
[2] Indoitu R, Orlovsky L and Orlovsky N 2012 Dust storms in Central Asia: spatial and temporal variations *J. Arid Environ.* **85** 62–70
[3] Knippertz P 2014 Meteorological aspects of dust storms *Mineral Dust: A Key Player in the Earth System* (Springer) pp 121–47
[4] Xi X and Sokolik I N 2015 Seasonal dynamics of threshold friction velocity and dust emission in Central Asia *J. Geophys. Res.* **120** 1536–64
[5] Li X, Juan Zhang Y, Gao H and Ding T 2022 Extreme cold wave in early November 2021 in China and the influences from the meridional pressure gradient over East Asia *Adv. Clim. Change Res.* **13** 797–802
[6] Zhang X, Tao H and Zheng Y 2022 Study on diagnosis weather process and flight impact of heavy snowfall in Northeast China "11/2021" *J. Geosci. Environ. Prot.* **10** 170–83
[7] Gao K, Wang J, Chen D, Hu W, Zhang Y, Duan A and Zhang X 2023 Synoptic climate settings and moisture supply for the extreme heavy snowfall in Northern China during 6–8 November 2021 *J. Meteorol. Res.* **37** 75–89
[8] Jiang J and Zhou T 2023 Agricultural drought over water-scarce Central Asia aggravated by internal climate variability *Nat. Geosci.* **16** 154–61
[9] Sayer A M, Munchak L A, Hsu N C, Levy R C, Bettenhausen C and Jeong M J 2014 Modis collection 6 aerosol products: comparison between aqua's e-deep blue, dark target and "merged" data sets and usage recommendations *J. Geophys. Res.* **119** 965–13
[10] Steinfeld D and Pfahl S 2019 The role of latent heating in atmospheric blocking dynamics: a global climatology *Clim. Dyn.* **53** 6159–80
[11] Steinfeld D 2021 *ConTrac—Contour Tracking* (Github) (available at: https://github.com/steidani/ConTrack)
[12] Ali S M, Martius O and Röthlisberger M 2021 Recurrent Rossby wave packets modulate the persistence of dry and wet spells across the globe *Geophys. Res. Lett.* **48** e2020GL091452
[13] Tuel A, Steinfeld D, Ali S M, Sprenger M and Martius O 2022 Large-scale drivers of persistent extreme weather during early summer 2021 in Europe *Geophys. Res. Lett.* **49** e2022GL099624
[14] Röthlisbergera M, Frossard L, Bosart L F, Keyser D and Martius O 2019 Recurrent synoptic-scale Rossby wave patterns and their effect on the persistence of cold and hot spells *J. Clim.* **32** 3207–26
[15] Szapiro N and Cavallo S 2018 TPVTrack v1.0: a watershed segmentation and overlap correspondence method for tracking tropopause polar vortices *Geosci. Model Dev.* **11** 5173–87
[16] Hakim G J 2000 Climatology of coherent structures on the extratropical tropopause *Mon. Weather Rev.* **128** 385–406
[17] Hakim G J and Canavan A K 2005 Observed cyclone-anticyclone tropopause vortex asymmetries *J. Atmos. Sci.* **62** 231–40

[18] Cavallo S M and Hakim G J 2009 Potential vorticity diagnosis of a tropopause polar cyclone *Mon. Weather Rev.* **137** 1358–71
[19] Papritz L, Rouges E, Aemisegger F and Wernli H 2019 On the thermodynamic preconditioning of arctic air masses and the role of tropopause polar vortices for cold air outbreaks from Fram Strait *J. Geophys. Res. Atmos.* **124** 11033–50
[20] Biernat K A, Bosart L F and Keyser D 2021 A climatological analysis of the linkages between tropopause polar vortices, cold pools and cold air outbreaks over the central and eastern United States *Mon. Weather Rev.* **149** 189–206
[21] Lillo S P, Cavallo S M, Parsons D B and Riedel C 2021 The role of a tropopause polar vortex in the generation of the January 2019 extreme arctic outbreak *J. Atmos. Sci.* **78** 2801–21
[22] Harris I, Osborn T J, Jones P and Lister D 2020 Version 4 of the CRU TS monthly high-resolution gridded multivariate climate dataset *Sci. Data* **7** 109
[23] Gruber A, Scanlon T, Van Der Schalie R, Wagner W and Dorigo W 2019 Evolution of the ESA CCI soil moisture climate data records and their underlying merging methodology *Earth Syst. Sci. Data* **11** 717–39
[24] Preimesberger W, Scanlon T, Su C H, Gruber A and Dorigo W 2021 Homogenization of structural breaks in the global ESA CCI soil moisture multisatellite climate data record *IEEE Trans. Geosci. Remote Sens.* **59** 2845–62
[25] Didan K and Huete A (MODAPS SIPS) 2015 *MOD13C2 MODIS/Terra Vegetation Indices Monthly L3 Global 0.05Deg CMG* (https://doi.org/10.5067/MODIS/MOD13C2.006)
[26] Hirschi M, Mueller B, Dorigo W and Seneviratne S I 2014 Using remotely sensed soil moisture for land-atmosphere coupling diagnostics: the role of surface vs. root-zone soil moisture variability *Remote Sens. Environ.* **154** 246–52
[27] Uzhydromet 2021 Information on non-seasonal dust haze events due to strong winds (available at: https://hydromet.uz/ru/node/1039)
[28] Wheeler D D, Harvey V L, Atkinson D E, Collins R L and Mills M J 2011 A climatology of cold air outbreaks over North America: WACCM and ERA-40 comparison and analysis *J. Geophys. Res. Atmos.* **116** D12107
[29] Winters A C and Martin J E 2016 Synoptic and mesoscale processes supporting vertical superposition of the polar and subtropical jets in two contrasting cases *Q. J. R. Meteorol. Soc.* **142** 1133–49
[30] Madonna E, Wernli H, Joos H and Martius O 2014 Warm conveyor belts in the ERA-interim dataset (1979–2010). Part I: climatology and potential vorticity evolution *J. Clim.* **27** 3–26
[31] Pfahl S, Schwierz C, Croci-Maspoli M, Grams C M and Wernli H 2015 Importance of latent heat release in ascending air streams for atmospheric blocking *Nat. Geosci.* **8** 610–4
[32] Cavallo S M and Hakim G J 2010 Composite structure of tropopause polar cyclones *Mon. Weather Rev.* **138** 3840–57
[33] Hanna E, Cropper T E, Hall R J and Cappelen J 2016 Greenland blocking index 1851–2015: a regional climate change signal *Int. J. Climatol.* **36** 4847–61
[34] Woollings T J, Hoskins B, Blackburn M and Berrisford P 2008 A new Rossby wave-breaking interpretation of the North Atlantic Oscillation *J. Atmos. Sci.* **65** 609–26
[35] Woollings T, Hannachi A and Hoskins B 2010 Variability of the North Atlantic eddy-driven jet stream *Q. J. R. Meteorol. Soc.* **136** 856–68
[36] Masato G, Hoskins B J and Woollings T 2013 Wave-breaking characteristics of Northern Hemisphere winter blocking: a two-dimensional approach *J. Clim.* **26** 4535–49
[37] Madonna E, Li C, Grams C M and Woollings T 2017 The link between eddy-driven jet variability and weather regimes in the North Atlantic–European sector *Q. J. R. Meteorol. Soc.* **143** 2960–72
[38] Thompson D W J and Wallace J M 2001 Regional climate impacts of the Northern Hemisphere annular mode *Science* **293** 85–89
[39] Walsh J E, Phillips A S, Portis D H and Chapman W L 2001 Extreme cold outbreaks in the United States and Europe, 1948–99 *J. Clim.* **14** 2642–58
[40] Jeong J H and Ho C H 2005 Changes in occurrence of cold surges over east Asia in association with Arctic Oscillation *Geophys. Res. Lett.* **32** 1–4
[41] Yu Y, Ren R and Cai M 2015 Dynamic linkage between cold air outbreaks and intensity variations of the meridional mass circulation *J. Atmos. Sci.* **72** 3214–32
[42] Xi X and Sokolik I N 2015 Dust interannual variability and trend in Central Asia from 2000 to 2014 and their climatic linkages *J. Geophys. Res.* **120** 12175–97
[43] Xi X 2023 On the geomorphic, meteorological and hydroclimatic drivers of the unusual 2018 early summer salt dust storms in Central Asia *J. Geophys. Res. Atmos.* **128** e2022JD038089
[44] Hunt K M R, Turner A G and Shaffrey. L C 2018 The evolution, seasonality and impacts of western disturbances *Q. J. R. Meteorol. Soc.* **144** 278–90
[45] Rana S, Renwick J, McGregor J and Singh A 2018 Seasonal prediction of winter precipitation anomalies over central Southwest Asia: a canonical correlation analysis approach *J. Clim.* **31** 727–41
[46] Barlow M, Cullen H and Lyon B 2002 Drought in Central and Southwest Asia: La Niña, the warm pool and Indian Ocean precipitation *J. Clim.* **15** 697–700
[47] Hoerling M and Kumar A 2003 The perfect ocean for drought *Science* **299** 691–4
[48] Trigo R M, Gouveia C M and Barriopedro D 2010 The intense 2007–2009 drought in the Fertile Crescent: Impacts and associated atmospheric circulation *Agric. For. Meteorol.* **150** 1245–57
[49] Hoell A, Funk C and Barlow M 2014 The regional forcing of Northern hemisphere drought during recent warm tropical west Pacific Ocean La Niña events *Clim. Dyn.* **42** 3289–311
[50] Barlow M and Hoell A 2015 Drought in the middle east and central-southwest Asia during winter 2013/14 *Bull. Am. Meteorol. Soc.* **96** S71–S76
[51] Hoell A, Barlow M, Xu T and Zhang T 2018 Cold season southwest Asia precipitation sensitivity to El Niño-Southern Oscillation events *J. Clim.* **31** 4463–82
[52] Hoell A, Funk C and Barlow M 2014 La Niña diversity and northwest Indian Ocean rim teleconnections *Clim. Dyn.* **43** 2707–24
[53] Weller E, Ki Min S, Cai W, Zwiers F W, Hee Kim Y and Lee D 2016 Human-caused Indo-Pacific warm pool expansion *Sci. Adv.* **2** e1501719
[54] Zscheischler J *et al* 2020 A typology of compound weather and climate events *Nat. Rev. Earth Environ.* **1** 333–47
[55] Takaya K and Nakamura H 2005 Mechanisms of intraseasonal amplification of the cold Siberian high *J. Atmos. Sci.* **62** 4423–40
[56] Takaya K and Nakamura H 2013 Interannual variability of the East Asian winter monsoon and related modulations of the planetary waves *J. Clim.* **26** 9445–61
[57] Won Park T, Ho C H and Deng Y 2014 A synoptic and dynamical characterization of wave-train and blocking cold surge over East Asia *Clim. Dyn.* **43** 753–70
[58] Geng T, Jia F, Cai W, Wu L, Gan B, Jing Z, Li S and McPhaden M J 2023 Increased occurrences of consecutive La Niña events under global warming *Nature* **619** 774–81